4386 *Chem. Mater.* **2010,** *22,* 4386–4391
DOI:10.1021/cm100440p

CHEMISTRY OF MATERIALS
Article

Probing Local Dipoles and Ligand Structure in $BaTiO_3$ Nanoparticles

Katharine Page,*,† Thomas Proffen,† Markus Niederberger,‡ and Ram Seshadri§

†*Los Alamos National Laboratory, LANSCE-LC, MS H805, Los Alamos, New Mexico 87545,* ‡*Department of Materials, ETH Zürich, 8093 Zürich, Switzerland, and* §*Materials Department, University of California, Santa Barbara, California 93106*

Received February 11, 2010. Revised Manuscript Received June 29, 2010

Improved routes for the preparation of nanoparticles, in conjunction with the development of more sophisticated structural probes for nanostructured materials, allows questions to be addressed regarding fundamental size limits on material properties. The property addressed here is structural off-centering, the molecular basis for the existence of switchable dipoles in polar materials, and whether it is turned off when particles become very small. This is probed using neutron scattering in a sample of free-standing, capped nanoparticles of the canonical perovskite ferroelectric, $BaTiO_3$, with sizes near 5 nm. The structure, analyzed in reciprocal and real space, reveals the atomic correlations of the nanoparticle oxide and the capping benzyloxy ligand groups, and allows careful comparison with the structure of bulk $BaTiO_3$. Even at these very small sizes, Ti is locally strongly off-centered, despite presenting cubic Bragg scattering.

Introduction

Since the concurrent multiple discoveries of its polar behavior in the 1940s, perovskite $BaTiO_3$ has become one of the most extensively studied functional materials[1,2] as a consequence of its high dielectric constant and room temperature ferroelectric behavior. $BaTiO_3$ finds uses in a number of applications, including ceramic, thin film, and multilayer capacitors,[3] and more recently, composite multiferroic architectures.[4] The material takes on four crystallographic phases, each with a distinct dielectric behavior. Changes in symmetry arise from the displacement of Ti atoms from the center of the oxygen octahedra, giving rise to spontaneous polarization. The ground state crystal structure is rhombohedral *R*3*m* with Ti displacements in the [111] direction. Between 183 and 298 K, the crystallographic phase is orthorhombic *Amm*2 with polarization along [011]. At room temperature, $BaTiO_3$ has a tetragonal *P*4*mm* crystal structure, with [001] polarization. Above 393 K, $BaTiO_3$ is paraelectric, with cubic $Pm\bar{3}m$ crystal structure.[1,5] Panels a, b, c, and d of Figure 1 show TiO_6 octahedra in different symmetries.

Ferroelectricity is frequently suppressed in $BaTiO_3$ architectures with one or more diminished dimensions (in thin films,[6−8] nanowires,[9] and nanoparticles[10]) due to reduced structural coherence. Many factors are thought to affect the nature of ferroelectricity in these systems, including molecular adsorbates[9] and substrate induced strain,[11] while factors such as compositional variation and processing-related defects are known to influence $BaTiO_3$ powders and ceramics.[12,13] Nonetheless, critical size effects will define the extent to which these materials can be incorporated into future generations of electronic devices and are of great fundamental interest. Accordingly, there have been many efforts at establishing the nature of ferroelectricity at small sizes. Density functional calculations predict that ferroelectricity in $PbTiO_3$ is robust to a few unit cells.[14,15] Recent experiments on thin $PbTiO_3$ grown on (001) $SrTiO_3$ substrates[16] and on $(BaTiO_3)_n(SrTiO_3)_m$ architecture[17] support this experimentally. The availability of high quality oxide nanoparticles has enabled the study of size effects in a number of ferroelectric materials, minus the effect of substrate or support.[18−20] Free powders, in contrast to thin films,

*To whom correspondence should be addressed. E-mail: kpage@lanl.gov.

(1) Megaw, H. D. *Ferroelectricity in Crystals*; Methuen: London, 1957.
(2) Lines, M. E.; Glass, A. M. *Principles and Applications of Ferroelectrics and Related Materials*; Clarendon: Oxford, U.K., 1977.
(3) Scott, J. F. *Science* **2007**, *315*, 954–959.
(4) Zheng, H.; et al. *Science* **2004**, *303*, 661–663.
(5) Kwei, G. H.; Lawson, A. C.; Billinge, S. J. L.; Cheong, S.-W. *J. Phys. Chem.* **1993**, *97*, 2368–2377.
(6) Shaw, T. M.; Trolier-McKinstry, S.; McIntyre, P. C. *Annu. Rev. Mater. Sci.* **2000**, *30*, 263–298.
(7) Ahn, C. H.; Rabe, K. M.; Triscone, J.-M. *Science* **2004**, *303*, 488–491.
(8) Dawber, M.; Rabe, K. M.; Scott, J. F. *Rev. Mod. Phys.* **2005**, *77*, 1083–1130.
(9) Spanier, J. E.; Kolpak, A. M.; Urban, J. J.; Grinberg, I.; Ouyang, L.; Yun, W. S.; Rappe, A. M.; Park, H. *Nano Lett.* **2006**, *6*, 735–739.
(10) Tanaka, M.; Makino, Y. *Ferroelectrics Lett.* **1998**, *24*, 13–23.
(11) Choi, K. J.; Biegalski, M.; Li, Y. L.; Sharan, A.; Schubert, J.; Uecker, R.; Reiche, P.; Chen, Y. B.; Pan, X. Q.; Gopalan, V.; Chen, L.-Q.; Schlom, D. G.; Eom, C. B. *Science* **2004**, *306*, 1005–1009.
(12) Frey, M. H.; Payne, D. A. *Phys. Rev. B* **1996**, *54*, 3158–3168.
(13) Lee, S.; Liu, Z. -K.; Kim, M.-H.; Randall, C. A. *J. Appl. Phys.* **2007**, *101*, 054119.
(14) Junquera, J.; Ghosez, P. *Nature* **2003**, *422*, 506–509.
(15) Spaldin, N. A. *Science* **2004**, *304*, 1606–1607.
(16) Fong, D. D.; Stephenson, G. B.; Streiffer, S. K.; Eastman, J. A.; Auciello, O.; Fuoss, P. H.; Thompson, C. *Science* **2004**, *304*, 1650–1653.
(17) Tenne, D. A.; et al. *Science* **2006**, *313*, 1614–1616.
(18) Petkov, V.; Gateshki, M.; Niederberger, M.; Ren, Y. *Chem. Mater.* **2006**, *18*, 814–821.
(19) Smith, M. B.; Page, K.; Siegrist, T.; Redmond, P. L.; Walter, E. C.; Seshadri, R.; Brus, L. E.; Steigerwald, M. L. *J. Am. Chem. Soc.* **2008**, *130*, 6955–6963.
(20) Petkov, V.; Buscaglia, V.; Buscaglia, M. T.; Zhao, Z.; Ren, Y. *Phys. Rev. B* **2008**, *78*, 054107.

 Published on Web 07/16/2010

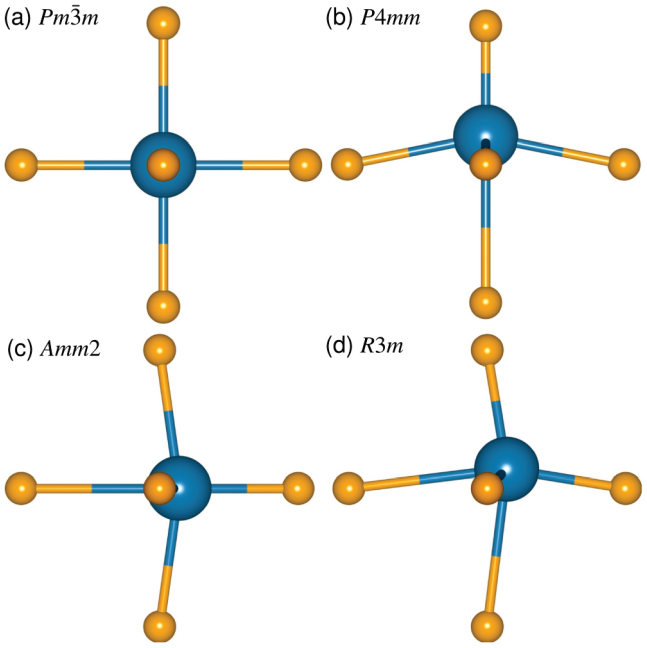

Figure 1. Depictions of TiO_6 octahedra in the (a) cubic, (b) tetragonal, (c) orthorhombic, and (d) rhombohedral structures. In b, c, and d, Ti displacements have been exaggerated for clarity.

allow a detailed description of crystal structure to be obtained, including all internal coordinates.

Separately, an important concern to emerge in recent years is the nanostructure problem.[23] Complete atom-by-atom descriptions of nanostructure are confined to the rare instance of a crystallized nanoparticle superlattice.[21] In recent years, the pair distribution function (PDF) analysis of total X-ray or neutron scattering has emerged as a powerful tool in the arsenal of nanostructure analysis methods. The PDF includes contributions from Bragg and diffuse scattering components, and while the former is very powerful in establishing those aspects of the structure that are well-correlated, the latter provides detailed local structure information.[22] The great strength of the PDF with respect to this study lies in directly probing atom−atom distances. The roots of the technique lie in the study of liquid and amorphous materials but, over the last 20 years, have found increasing application in describing the departure of local atomic structure from average, crystallographic structure in bulk materials, and more recently, in the study of nanomaterials.[18−20,24−32] There have been few neutron PDF studies of nanomaterials[33,34] due to sample size requirements and significant incoherent neutron scattering from hydrogen atoms inherent to capping or stabilizing layers.

Here, we present the room temperature structure of 5 nm $BaTiO_3$ particles, with bulk $BaTiO_3$ as a reference for comparison, using Rietveld and PDF analyses of high momentum-transfer time-of-flight neutron scattering data. The analysis reveals the detailed structure, including accurate metal−oxygen distances and the presence of the benzyloxy ligand group. This work extends our previous X-ray local structure studies of 26 to 70 nm $BaTiO_3$ particles[19] into a new size regime and reveals features of Ti−O distances that are not well probed with X-ray scatttering.

Experimental Section

Nominally spherical $BaTiO_3$ nanoparticles were prepared via a nonhydrolytic and halide-free route from barium metal and titanium isopropoxide in anhydrous benzyl alcohol.[35] Barium metal and titanium isopropoxide were dissolved in anhydrous benzyl alcohol at low temperatures and reacted in an autoclave at 200 °C for 48 h to form pure, stoichiometric, and homogeneous $BaTiO_3$ nanocrystals. A bulk $BaTiO_3$ standard was prepared by ceramic methods for comparison.

Neutron scattering data were collected on the NPDF diffractometer[36] at the Lujan Center at Los Alamos National Laboratory for powders of bulk $BaTiO_3$ (2 g) and nanoparticle $BaTiO_3$ (0.7 g) contained in vanadium cans. Data were collected at room temperature for 4 h for the bulk sample and 9 h for the nanoparticles.

The GSAS-EXPGUI suite of programs were used to complete the Rietveld refinement of the data.[37] Fits were made using a tetragonal *P*4*mm* model for the bulk data, and both tetragonal *P*4*mm* and cubic $Pm\bar{3}m$ models for the nanoparticle data. Scale factor, profile parameters, lattice parameters, atomic coordinates, and isotropic atomic displacement parameters were refined in the analysis. For the nanoparticle Rietveld analysis the refinement of atom positions was unstable, and the parameters were fixed to the refined bulk values.

Routine steps were followed in order to extract the experimental PDF $G(r)$ from the bulk $BaTiO_3$ data. The data were corrected for instrument background, incident neutron spectrum, absorption, and multiple scattering, and finally normalized using the program PDFgetN.[38] The extraction of the experimental PDF $G(r)$ for the nanoparticle sample required additional steps due to incoherent scattering contributions from hydrogen atoms in the particle ligand to the experimental total

(21) Jadzinsky, P. D.; Calero, G.; Ackerson, C. J.; Bushnell, D. A.; Kornberg, R. D. *Science* **2008**, *318*, 430–433.
(22) Egami, T.; Billinge, S. J. L. *Underneath the Bragg-Peaks: Structural Analysis of Complex Materials*; Elsevier: New York, 2003.
(23) Billinge, S. J. L.; Levin, I. *Science* **2007**, *316*, 561–565.
(24) McKenzie, D. R.; Davis, C. A.; Cockayne, D. J. H.; Muller, D. A.; Vassallo, A. M. *Nature* **1992**, *335*, 622–624.
(25) Szczygielska, A.; Jablonska, A.; Burian, A.; Dore, J. C.; Honkimaki, V.; Nagy, J. B. *Acta Phys. Pol., A* **2000**, *98*, 611–617.
(26) Zhang, H.; Gilbert, B.; Huang, F.; Banfield, J. F. *Nature* **2003**, *424*, 1025–1029.
(27) Gilbert, B.; Huang, F.; Zhang, H.; Waychunas, G. A.; Bandield, J. F. *Science* **2004**, *305*, 651–654.
(28) Gateshki, M.; Hwang, S.-J.; Park, D. H.; Ren, Y.; Petkov, V. *J. Phys. Chem. B* **2004**, *108*, 14956–14963.
(29) Masadeh, A. S.; Bozin, E. S.; Farrow, C. L.; Paglia, G.; Juhas, P.; Billinge, S. J. L.; Karkamkar, A.; Kanatzidis, M. G. *Phys. Rev. B* **2007**, *76*, 115413.
(30) Bedford, N.; Dablemont, C.; Viau, G.; Chupas, P.; Petkov, V. *J. Phys. Chem. C* **2007**, *111*, 18214–18219.
(31) Pradhan, S. K.; Mao, Y.; Wong, S. S.; Chupas, P.; Petkov, V. *Chem. Mater.* **2007**, *19*, 6180–6186.
(32) Chupas, P. J.; Chapman, K. W.; Jennings, G.; Lee, P. L.; Grey, C. P. *J. Am. Chem. Soc.* **2007**, *129*, 13822–13824.
(33) Page, K.; Proffen, Th.; Terrones, H.; Terrones, M.; Lee, L.; Yang, Y.; Stemmer, S.; Seshadri, R.; Cheetham, A. K. *Chem. Phys. Lett.* **2004**, *393*, 385–388.
(34) Ojeda-May, P.; Terrones, M.; Terrones, H.; Hoffman, D.; Proffen, Th.; Cheetham, A. K. *Diamond Relat. Mater.* **2007**, *16*, 473–476.
(35) Niederberger, M.; Garnweitner, G.; Pinna, N.; Antonietti, M. *J. Am. Chem. Soc.* **2004**, *126*, 9120–9126.
(36) Proffen, T.; et al. *Appl. Phys. A: Mater. Sci. Process.* **2002**, *74*, S163–S165.
(37) Toby, B. H. *J. Appl. Crystallogr.* **2001**, *34*, 210–213.
(38) Peterson, P. F.; Gutmann, M.; Proffen, T.; Billinge, S. J. L. *J. Appl. Crystallogr.* **2000**, *33*, 1192.

neutron scattering structure function $S(Q)$. Incoherent inelastic scattering contributions were removed from beneath the normalized distinct scattering signal, and the scattering contribution expected from coherent inelastic scattering was reintroduced to the data by using the bulk $S(Q)$ data as a reference. This semiempirical data correction procedure and its effects on the experimental pair distribution function are detailed elsewhere.[39]

Full profile PDF structure refinements were carried out for the bulk and 5 nm $BaTiO_3$ $G(r)$s using the program PDFgui.[40] The nanoparticle oxide phase was modeled with both cubic and tetragonal, and metrically cubic unit cells with the Ti atoms displaced along the [001] and [111] directions, respectively. Lattice parameters, isotropic atomic displacement parameters, and atom positions were refined for each model. Calibration of the NPDF instrument using standard samples provided parameters describing the PDF dampening envelope due to instrument resolution and PDF peak broadening due to intensity noise.[41] The analysis of nanoparticle data utilized an additional parameter in PDFgui, designed to deduce the average spherical particle diameter from additional decay in the experimental PDF.

Results and Discussion

Transmission Electron Microscopy (TEM) images presented in Supporting Information, Figure S1, show the particles are single crystalline, nominally spherical, and near 5 nm in average diameter. The inset in the upper left corner of the figure shows an elongated particle. Elliptical nanoparticle envelope functions are not implemented in the data refinement program PDFgui. Anisotropic spheroids and particle size distribution affect the envelope function minimally in the size range studied here.[42,43] Our quantitative results for the structural phases were obtained by refinement of the data below 30 Å and are expected to be unaffected by the occurrence of anisotropy in some fraction of particles. Thermogravimetric analysis suggested that roughly 3.7% of the total mass is lost on heating to 400 °C, attributable to the physisorbed species (Figure S2, Supporting Information). Between 400 and 1200 °C, a further mass loss of 13.7% corresponding to the complete calcination of chemisorbed organic capping groups was observed. From this latter mass loss, a mass ratio of capping group to $BaTiO_3$ of 0.16 is obtained, corresponding to a mole ratio of 0.35.

We first examine the structure of bulk and nanoparticle $BaTiO_3$ in reciprocal space using Rietveld refinement. Room temperature neutron diffraction data for bulk $BaTiO_3$ was fit with the tetragonal *P4mm* perovskite structure. The refinement result is shown in Figure 2a, and is unambiguous with regard to the choice of space group. Two models were attempted in the analysis of the nanoparticle data: in panel b, the tetragonal *P4mm* model and in panel c, the cubic $Pm\bar{3}m$ model. The data are

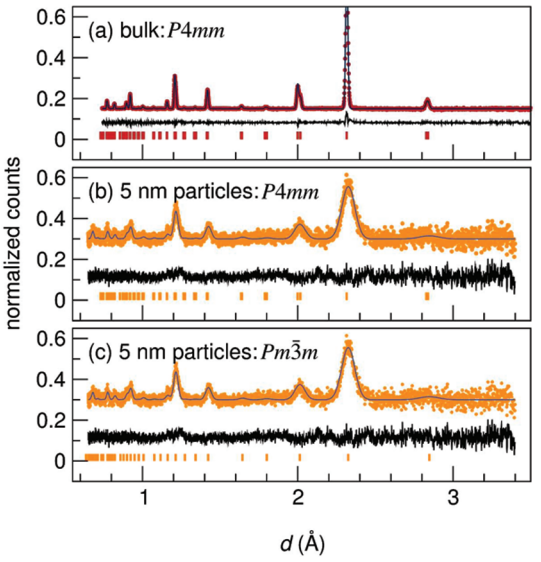

Figure 2. Rietveld profile analysis (data as points, fits and differences as lines, and expected peak positions marked with vertical markers) for (a) bulk $BaTiO_3$ and (b,c) 5 nm $BaTiO_3$. The 5 nm particles were fit to the room temperature tetragonal *P4mm* structure and to the cubic high temperature $Pm\bar{3}m$ structure.

shown with refined background removed. For the nanoparticle data, the broadening of diffraction peaks is significant, making the models indistinguishable. However, refinement of atomic positions in the *P4mm* model was not stable for nanoparticle data; therefore, we conclude that the average structure, as revealed by Bragg scattering, is cubic. Some results of Rietveld analyses of Bragg scattering from bulk and nanoparticles are presented in Table 1.

The total neutron scattering structure function $S(Q)$ is displayed for bulk $BaTiO_3$ in Figure 3a. The corresponding PDF $G(r)$ is displayed in panel b. For the bulk data, the decay in correlation peak intensity is determined by instrument resolution and intensity noise. The experimental $S(Q)$ for the nanoparticles is shown in Figure 3c, and this was used for conversion to $G(r)$ in panel d. In the nanoparticle PDF, the extent of atom−atom correlations is influenced by the particle diameter, where the PDF approaches zero. A quantitative analysis of $G(r)$ yields a particle size of 4.7(1) nm, in good agreement with Scherrer broadening analysis of the diffraction data and the TEM images in Supporting Information, Figure S1. We refer to the nanoparticle sample as 5 nm particles.

PDF data from bulk $BaTiO_3$ at room temperature refines in the expected average tetragonal crystal structure (*P4mm*) as displayed in Figure 4a, particularly for r ranges larger than 4 Å. However, as seen in the inset of this figure, the nearest neighbor Ti−O correlations are not described by the model. At room temperature, bulk $BaTiO_3$ locally retains rhombohedral symmetry, with the Ti atom displacing toward one of the faces of its octahedral coordination polyhedron. The *R3m* fit is compared with the *P4mm* fit in the inset. The persistence of the lowest-temperature distortion mode at a very local scale, even at room temperature, has been noted in a number of studies in keeping with the order−disorder behavior of

(39) Page, K.; White, C. E.; Estell, E. G.; Llobet, A.; Proffen, Th., submitted for publication.
(40) Farrow, C. L.; et al. *J. Phys.: Condens. Matter* **2007**, *19*, 335219.
(41) Toby, B. H.; Egami, T. *Acta Crystallogr., Sect. A* **1992**, *48*, 336–346.
(42) Kodama, K.; Iikubo, S.; Taguchi, T.; Shamoto, S. *Acta Crystallogr., Sect. A* **2006**, *62*, 444–453.
(43) Gilbert, B. *J. Appl. Crystallogr.* **2008**, *41*, 554–562.

Table 1. Results of Rietveld and PDF (0.7 to 15 Å Range) Analysis of Time of Flight Neutron Diffraction Data for Bulk and 5 nm $BaTiO_3$[a]

	bulk (*P*4*mm*)		5 nm (*P*4*mm*)		5 nm (*Pm*3*m*)	
	Rietveld	PDF	Rietveld	PDF	Rietveld	PDF
a (Å)	3.99836(2)	3.9991(1)	4.0115(9)	4.005(3)	4.0261(3)	4.025(1)
c (Å)	4.03288(4)	4.0456(3)	4.057(2)	4.072(7)		
c/*a*	1.0086	1.011	1.0113	1.0167		
volume (Å^3)	64.473	64.700	65.30	65.315	65.261	65.256
z(Ti)	0.5135(9)	0.4855(5)	0.5135	0.53(1)		
z(O1)	−0.0219(5)	0.0265(4)	−0.0219	0.00(1)		
z(O2)	0.488(1)	0.5160(7)	0.488	0.51(1)		
U_{iso}, Ba (Å^2)	0.005(1)	0.004(1)	0.010(1)	0.003(2)	0.006(1)	0.006(2)
U_{iso}, Ti (Å^2)	0.0073(2)	0.0056(1)	0.009(1)	0.007(3)	0.011(1)	0.010(2)
U_{iso}, O (Å^2)	0.008(1)	0.007(1)	0.010(1)	0.012(1)	0.011(1)	0.012(1)
R_w (%)	3.49	5.72	1.55	15.7	1.55	16.1
1 × Ti−O (Å)	1.874(2)	1.857(4)	1.8849(9)	1.9(1)		
4 × Ti−O (Å)	2.0018(3)	2.0034(4)	2.0084(4)	2.005(6)		
1 × Ti−O (Å)	2.159(4)	2.189(4)	2.172(1)	2.2(1)		
4 × Ba−Ti (Å)	3.441(2)	3.443(1)	3.4557(7)	3.42(3)		
4 × Ba−Ti (Å)	3.504(2)	3.511(1)	3.5194(7)	3.56(3)		

[a] Fits were made using a tetragonal *P*4*mm* model for the bulk data and both tetragonal *P*4*mm* and cubic $Pm\bar{3}m$ models for the nanoparticle data. Refined parameters (lattice parameters *a* and *c*, *z* atomic coordinates, and isotropic atomic displacement parameters U_{iso}) are presented with last-place uncertainties in parentheses. For the nanoparticle Rietveld analysis, the positions of atoms were held fixed to the refined bulk values.

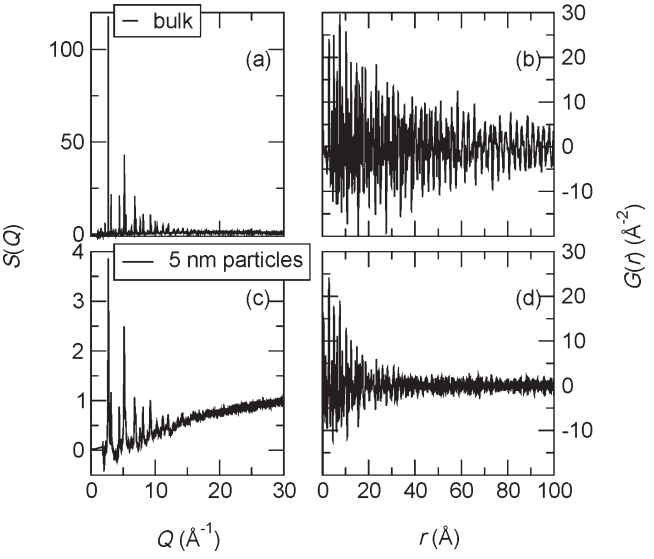

Figure 3. Comparison of the neutron scattering $S(Q)$ (a,c) and $G(r)$ (b,d) for bulk $BaTiO_3$ and 5 nm $BaTiO_3$ particles, respectively. The data in c are shown after empirical background subtraction for inelastic scattering. In d, the nanoparticle $G(r)$ is shown scaled by the factor refined in PDF analysis. Note the differences in the intensity scales and peak broadening between panels a and c and in the decay of the high-*r* $G(r)$ signal in b and d, between the bulk and nanoparticle data.

the phase transition and in agreement with detailed models derived from various structural techniques.[2] In particular, a previous neutron PDF study of bulk $BaTiO_3$ phases indicated negligible changes in nearest neighbor atom−atom distances above and below crystallographic phase transitions.[44] The tetragonal crystal structure is the result of averaging [111] displacements of octahedral Ti over all four $+z$ directions.

The results of modeling the 5 nm particle PDF are shown in Figure 4b. After initial long-range refinement, the particle size was fixed to 4.7(1) nm. The modeling of the nanoparticle data required the inclusion of a second phase, whose relative amount was refined, to describe the structure of ligands at the surface of the particle. This contribution was modeled with a rigid benzyl alcohol molecule (details provided in Supporting Information). Parameters refined for the molecule included a scale factor, model dimensions, and an overall isotropic atomic displacement parameter for the atoms of the molecule. Contributions from the *P*4*mm* perovskite oxide structure and from the molecular structure of benzyl alcohol are shown below the data and fit. The rigid benzyl alcohol molecule used in the model is presumably attached to the surface of the particle. PDF phase analysis yielded a benzyl alcohol to $BaTiO_3$ mole ratio of 0.17, roughly half the value of 0.35 suggested by thermogravimetric analysis. For 4.7 nm particles, a 0.35 mol ratio suggests approximately one capping molecule for every 15 Å^2 of nanoparticle surface. The mole ratio emerging from PDF analysis corresponds to a surface density of one capping molecule for every 40 Å^2 of nanoparticle surface. The reason for these discrepancies is unclear at this time. The mode of binding between the benzyloxy groups and the nanoparticles is consistent with the Ti atoms on the surface binding to the O on the benzyloxy capping group. The fine details of the surface structure of the nanoparticles and of the distance between Ti and O in the capping groups do not emerge from this study (the latter especially hindered by the overlap of Ti−O distances in the two phases).

The agreement factors from PDF analysis of the 5 nm particles suggest that the *P*4*mm* structure provides a better description of the data than the cubic $Pm\bar{3}m$ structure (Table 1). Unlike the situation with Rietveld analysis, internal coordinates and hence atom−atom distances can be reliably refined in the nanoparticle PDF, although these are found to correlate strongly with atomic displacement parameters. The overlap of atom−atom pairs from the two phases (oxide particle and capping group) in the low-*r* region prevent us from

(44) Kwei, G. H.; Billinge, S. J. L.; Cheong, S.-W.; Saxton, J. G. *Ferroelectrics* **1995**, *164*, 57–73.

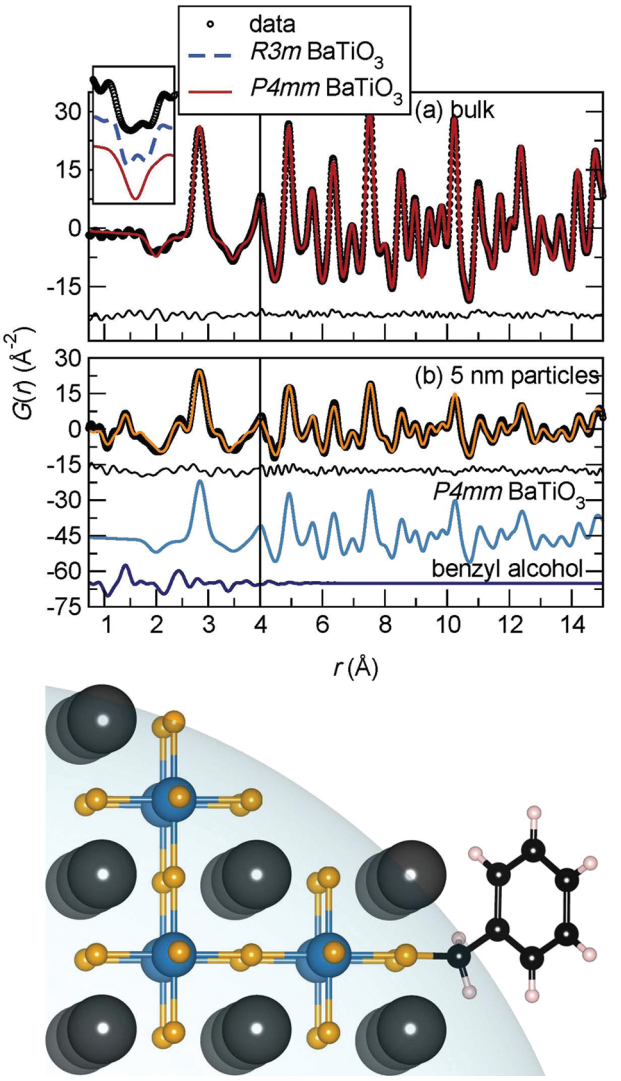

Figure 4. Neutron pair distribution function $G(r)$ analysis of (a) bulk and (b) 5 nm $BaTiO_3$. Experimental data are displayed as points and fits and differences with lines. In panel a, it is seen that bulk $BaTiO_3$ is well described by the *P4mm* structure, except for the nearest neighbor Ti−O distance near 2 Å displayed in the inset, which is split in a manner reminiscent of the structure of rhombohedral *R3m* rather than tetragonal *P4mm* $BaTiO_3$. The peak is negative because of the negative scattering length of Ti. The nanoparticle $G(r)$ is seen to require contributions from *P4mm* $BaTiO_3$ as well as benzyl alcohol to fit the experimental data. The schematic image below depicts part of the nanoparticle, near the surface, with a single capping benzyloxy group.

directly drawing conclusions about the presence of local rhombohedral distortions. However, rhombohedral distortions (Ti displacing along [111] directions) are not excluded by this study. In order to ensure that off-centering displacements are robust and persist in these small particles, the *r*-range dependence of Ti−O bond distances in tetragonal and pseudotetragonal $BaTiO_3$ models (Figure 5a), and in rhombohedral and pseudo-rhombohedral models (Figure 5b) have been compared with the experimental data. It is seen that refinements in these models are stable over a 10 Å to 30 Å range, with higher reliability in distances seen in models that involve metrically cubic unit cells but displacements of Ti toward an octahedral corner ([100] displacement) or toward the octahedral face ([111] displacement). In both cases, the

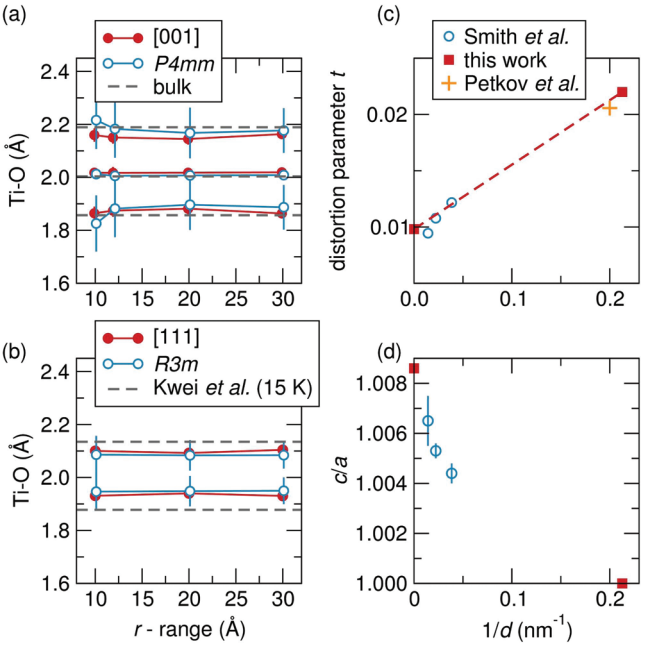

Figure 5. Verifying the robust off-centering of Ti within TiO_6 octahedra in 5 nm $BaTiO_3$. Panels a and b display the *r*-range dependence of Ti−O distances obtained from fitting the $G(r)$ to different models. In panel a, the three distances (1 long, 1 short, and 4 intermediate) were obtained from two different models, one a metrically cubic model with Ti displaced along [001] and the other the *P4mm* structure. Horizontal lines are distances from the room temperature PDF refinement of bulk $BaTiO_3$ performed over a range of 15 Å. In panel b, the two distances are from the refinement of a metrically cubic model with the Ti displaced along the [111] direction, compared with the rhombohedral *R3m* structure. Horizontal lines are the two distances obtained from the 15 K Rietveld refinement of bulk $BaTiO_3$ by Kwei et al.,[5] and panel c displays a distortion parameter, calculated as defined in the text and panel d the c/a ratio as a function of the inverse particle size. Data from this study are compared with data from Smith et al.[19] and Petkov et al.[18].

magnitude of the distortion compares closely with what is observed in bulk $BaTiO_3$. The results consistently show the Ti off-centering, no matter how we model. It is possible that both modes of Ti displacement exist in the nanoparticle, in keeping with the idea that vortices of the dipole can develop in nanophase ferroelectrics.[45]

In a previous X-ray scattering study of small $BaTiO_3$ particles, it was determined that while the smaller particles appear metrically more cubic at room temperature, the dipoles, or static displacements within them are actually larger.[19] The previous study focused on Ba−Ti distances which are more reliably obtained from X-ray scattering than Ti−O distances. Similar results have been obtained by Petkov et al.[18,20] who observed local tetragonal distortions and long-range (average) cubic structures. We define a distortion parameter t for tetragonal unit cells based on Ba−Ti distances as follows and plot it as a function of the inverse distance $1/d$ in Figure 5c with data taken from multiple studies.

$$t = \frac{(\mathrm{Ba-Ti})_{\mathrm{long}} - (\mathrm{Ba-Ti})_{\mathrm{short}}}{(\mathrm{Ba-Ti})_{\mathrm{long}} + (\mathrm{Ba-Ti})_{\mathrm{short}}}$$

This distortion parameter is seen to systematically increase as the particle size is decreased. The increased distortion should

(45) Naumov, I. I.; Bellaiche, L.; Fu, H. *Nature* **2004**, *432*, 737–740.

be compared with the difference between the shortest and longest Ti−O bond lengths in the short-range ($r < 10$ Å) PDF refinement. The refined values here match those found in bulk $BaTiO_3$ within experimental uncertainty. The rhombohedral models are less distorted than bulk (low temperature) $BaTiO_3$ because of greater degeneracy in local [111] displacements. The increased local distortion as measured by t is in contrast to the c/a ratio, which decreases with decreasing particle size as displayed in Figure 5d. Clearly, as size is decreased, local dipoles remain present, while dipole−dipole correlations decrease.

Larger local dipoles (greater extent of off-centering, as measured by t) within the unit cells may be explained with the expanded unit cell of the 5 nm particles: 65.3 Å^3 compared with the cell volume of bulk $BaTiO_3$ which is 64.7 Å^3 (Table 1).[19] The larger volume in small particles of many oxides is attributed to the spatial truncation of the electrostatic Madelung potential.[46] Several other factors may play a role. In $BaTiO_3$ thin films, ferroelectric properties have been enhanced through strain engineering,[11] and theoretical calculations on bare and molecule-covered $BaTiO_3$ nanowires indicate that ferroelectricity is stabilized by surface chemistry.[9] In addition, the ferroelectric properties of $BaTiO_3$ ceramics and powders are known to vary considerably with processing related defects[12] and nonstoichiometry.[13] How and to what extent these factors influence capped nanoparticles in the 5 nm regime is unknown, but it is hoped this work will engender investigation into these matters. Regardless of cause, the experimental finding of local tetragonal distortions in a powder of isolated nanoparticles in this size regime is an important observation.

(46) Perebienos, V.; Chan, S.-W.; Zhang, F. *Solid State Commun.* **2002**, *123*, 295–297.

Conclusions

We have used total scattering neutron pair distribution function analysis to reveal the picture of small $BaTiO_3$ particles being metrically more cubic, as a consequence of decreased dipole−dipole correlations, while retaining tetragonal distortion similar to bulk $BaTiO_3$ locally. The ability to perform such a study on capped, isolated nanoparticles allows comparisons to be made with other nanosystems including thin films and nanowires. Finally, the means to probe the complete structure of nanoparticles, including internal coordinates of the oxide and the capping organic functional group, has implications for a closer examination of other hybrid organic−inorganic systems and the roles size dependence, defect structure, surface chemistry, and other effects play in determining material properties in numerous functional nanosystems.

Acknowledgment. This work has benefited from the use of NPDF at the Lujan Center at Los Alamos Neutron Science Center, funded by the DOE Office of Basic Energy Sciences. Los Alamos National Laboratory is operated by Los Alamos National Security LLC under DOE contract DE-AC52-06NA25396. The National Science Foundation is acknowledged for support in the form of a Career Award to RS (grant DMR04-49354) and for an upgrade of the NPDF instrument at Los Alamos (grant DMR00-76488). We thank the National Science Foundation (DMR05-20415) for use of the MRSEC facilities.

Supporting Information Available: Details of incorporating the molecular phase in refinements, complete references 4 and 17, transmission electron microscopy images, and thermogravimentric analysis of the nanoparticle sample (PDF). This material is available free of charge via the Internet at http://pubs.acs.org/.